

Spectroscopy and dynamics of the dipole-bound state of acetaldehyde enolate

Roy D. Mead,^{a)} Keith R. Lykke, and W. C. Lineberger^{b)}

Department of Chemistry, University of Colorado and Joint Institute for Laboratory Astrophysics, University of Colorado and National Bureau of Standards, Boulder, Colorado 80309

J. Marks and John I. Brauman

Department of Chemistry, Stanford University, Stanford, California 94305

(Received 30 May 1984; accepted 31 July 1984)

Ultrahigh-resolution photodetachment spectroscopy of acetaldehyde enolate negative ion has revealed ~ 50 narrow resonances near threshold, corresponding to excitation to a diffuse state in which the electron is weakly bound by the field of the molecular dipole. A complete analysis of rotational transitions between the ground valence state and the excited dipole-bound state has been carried out, yielding spectroscopic constants and geometries for both states. In analogy to Rydberg states, the structure of the "neutral core" of the dipole-bound state is like that of the neutral radical. The dependence of autodetachment lifetimes upon the rotational quantum numbers of the dipole-bound state has been measured. Bound levels of the dipole-bound anion state are readily electric-field detached. The selection rules and dynamics of autodetachment from the dipole-bound state are discussed.

I. INTRODUCTION

In addition to conventional valence states, some negative ions also exhibit¹⁻⁴ novel bound states where the extra electron is bound primarily by interaction with the electric dipole moment of the neutral core. These "dipole-bound states" are characterized by the electron's small binding energy, diffuse wave function with large radius, and weak perturbation of the core. Theory predicts⁵ that *all* neutral molecules with dipole moments exceeding roughly 2 D will support such states, including species where no valence negative ion states exist. Dipole-bound states may be viewed as the next step beyond hydrogenic or Rydberg states; the binding is caused by an electric dipole field rather than by an electric monopole field. It is the combination of their ubiquity in real systems and the fundamental physical nature of the problem that make dipole-bound states important and interesting subjects for study.

The earliest theoretical work on binding of electrons in dipolar fields was done in 1947 by Fermi and Teller⁶ who report (without derivation) $0.639 ea_0$ (1.625 D) to be the *minimum* dipole moment required to support a bound state in a fixed dipolar field. Two years later Wightman⁷ derived this result by separating the Schrödinger equation in elliptic coordinates and finding the dipole moment at which the binding energy became zero. This early work was related to meson capture by hydrogen and was essentially unknown to molecular physicists, who rederived⁸ the result some 20 years later. Results were also published⁹ for excited states with different numbers of nodes and for states with angular momentum about the dipole axis.

The theory developed before 1970 was for fixed (or equivalently, infinitely massive) dipoles. The fixed-dipole treatment predicts an *infinite* number of bound states for moments greater than the critical value, similar to the result for a monopole field. More recent work by Garrett^{5,10} has

included the very important effects of rotation. Even in the ground rotational state, the critical moment increases when the nuclei are no longer fixed. In the ground rotational state whose *total* angular momentum is zero, the electron and dipole core may each have finite angular momentum and exert torque upon one another. This interaction raises the value for the minimum dipole moment and reduces the number of bound states to only a few. Garrett's calculations^{5,10} use a pseudopotential with the short-range cutoff adjusted to reproduce the electron affinity of the lowest dipole-bound state of some chosen reference species. The wave function and energy are then found by solving coupled radial equations. When parametrized to similar reference species, the theory¹¹ can be used to predict electron affinities of strongly dipolar closed-shell molecules, though experimental results for excited states are not available for comparison. Like the fixed-dipole models, this method neglects core penetration by the bound electron and predicts nodal structure different from *ab initio* molecular calculations.¹²

Quantum-chemical calculations^{12,13} on the binding of electrons by real (but nonrotating) diatomic molecules have been performed by several groups. The electronic structure they find is significantly different from that expected for a dipole consisting simply of point charges. The orbital of the dipole-bound electron must be orthogonal to the orbitals of the core, introducing nodal structure not seen in the point-charge system. The method obtains good agreement with experiment¹⁴ for ground-state binding energies of alkali-halide ions.

The existence of dipole-bound states is suggested by a number of experiments. Studies of electron scattering by polar molecules show strong resonances near zero energy. Wong and Schulz¹⁵ and Rohr and Linder¹⁶ suggest these resonances are caused by temporary electron capture into dipole-supported states lying in the continuum. Since many nonpolar molecules also show threshold resonances,¹⁷ these results are not conclusive evidence for dipole-bound states, even though they nevertheless may be participants in these

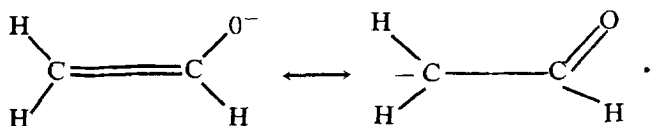
^{a)} Present address: Department of Chemistry, Stanford University, Stanford, Ca 94305.

^{b)} Faculty Fellow, University of Colorado, 1984.

scattering studies. Theoretical models¹⁸ have explained these resonances, and have shown a dipole moment need not be present for threshold resonances to exist.

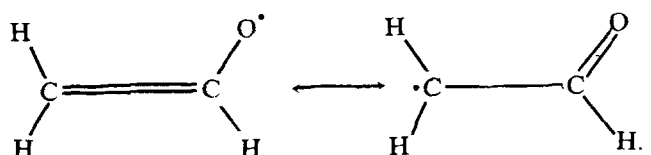
The most convincing experimental evidence for dipole-bound states has come from low-resolution photodetachment studies^{3,4} of highly polar enolate negative ions. Several of these compounds (which have dipole moments in the range of 2–4 D) were found to display resonances near threshold in their photodetachment cross sections. The resonances were interpreted as arising from optical excitation from the anion ground state to an upper “dipole supported” state, which subsequently decayed to the radical and a free electron. The data, taken in an ion-cyclotron-resonance spectrometer, do not show resolved structure within the broad (50 cm^{-1}) peaks at vibrational transitions. Without resolution of the underlying structure of the transitions, they could not unequivocally be assigned to dipole-bound states. These photodetachment experiments motivated the present work on acetaldehyde enolate negative ion.

This experimental evidence prompted extensive calculations on the electronic structure of the relevant states. The electronic structure of the neutral acetaldehyde enolate radical has been the subject of several *ab initio* calculations,^{19–21} and results have been obtained for the anion¹⁹ as well. Simple consideration of the resonance forms for the anion and neutral provide insight into this structure. The anion may be described by resonance between two forms:



The form on the left, with the negative charge located on the oxygen, is expected to make the predominant contribution to the hybrid, since primary carbon negative ions tend to be less stable than oxygen-centered anions.

Likewise, the radical has two resonance forms:



The form on the right gives the best description of the radical electronic structure, although resonance stabilization is not as important as for the negative ion.

Calculations also were performed for a dipole-bound state¹⁹ which should have a structure similar to that of the radical, since the bound electron will have very weak interaction with the core. Its very diffuse orbital will lie behind the positively charged CH_2 group, away from the negatively charged oxygen atom.

We have already published a brief note¹ showing a few of our results; in this paper, our observations are displayed in their entirety and we explain in detail the methods of analysis used and the results obtained. We shall discuss the apparatus used in the present studies, and proceed to examine the photodetachment cross section of acetaldehyde enolate negative ion at successively higher levels of resolution. As the

ability to resolve features progresses, even more detailed structure is observed. At first, vibrational structure is apparent, but eventually individual rotational states are resolved and the structure of the states of the anion are determined and compared with the radical structure. Finally, the binding energy of the dipole-bound state is determined, and the dynamics of autodetachment and electric-field detachment are discussed.

II. EXPERIMENTAL

A. Ion beam generation

Many aspects of the ion beam photodetachment apparatus have been described in detail in an earlier paper²² and will be discussed only briefly. An $\sim 2\text{ nA}$ beam of acetaldehyde enolate negative ions is formed by extracting the ions from a hot-cathode electric discharge containing approximately 0.1 Torr of acetaldehyde ($\text{H}_3\text{C}-\text{CHO}$), selecting mass m/e 43 with 90° sector magnet, and accelerating to 3 keV. Experiments on deuterated acetaldehyde enolate utilize 99% enriched $\text{D}_3\text{C}-\text{CDO}$, giving a strong peak at m/e 46 for photodetachment. The ion beam is then merged with the laser beam over a 30 cm path by means of electrostatic quadrupole deflectors.²³ The section of the apparatus where the beams are merged and the various particles are detected is shown in Fig. 1. The entire chamber in which the beams are merged is magnetically shielded and use of magnetically sus-

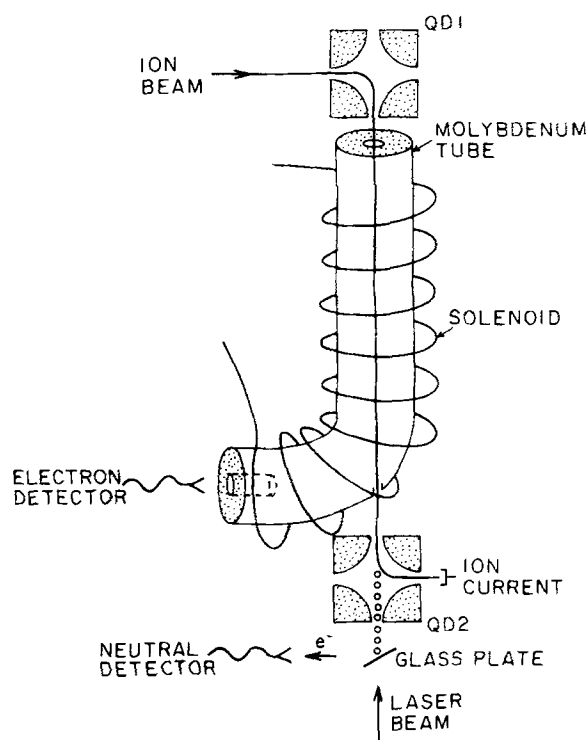


FIG. 1. View of the ion-beam optics, electron collector, and particle detectors used in the merged-beam photodetachment apparatus. The entire region shown is enclosed in magnetic shielding and is pumped to below 10^{-9} Torr. The ion beam is extracted from a hot cathode discharge, mass selected, and focused, and enters the region pictured from the upper left. The dye-laser beam used for photodetachment enters at the bottom of the figure. Quadrupole deflectors (Ref. 23) QD1 and QD2 are used to merge the ion beam with the laser beam.

ceptible materials has been avoided. After leaving the interaction region, the remaining ions and neutrals formed by photodetachment are separated electrostatically by a second quadrupole deflector. The photodetached neutrals pass directly through the second quadrupole deflector, strike a glass plate, and due to their high velocity (characteristic of the anions from which they were formed), produce secondary electrons which are detected by an electron multiplier. The pressure in the interaction region is typically 4×10^{-10} Torr.

B. Electron collection system

Collection and detection of the neutral photodetachment products is relatively straightforward, since they are produced as a high-energy collimated beam. Collection of the electrons produced by photodetachment is a much more difficult problem, especially if one wishes to discriminate against fast electrons so as to enhance threshold features in cross sections. Electrons are emitted by the photodetaching ions throughout the 30 cm long \times 1 mm diameter interaction volume. Very near threshold, these electrons have essentially the same speed and direction as the ion beam. An electron moving at this velocity has only about 40 meV kinetic energy in the lab frame, and is therefore easily influenced (intentionally or unintentionally) by weak electromagnetic fields. Higher energy electrons can have speeds greater or less than the ion beam, and can be emitted with some component of velocity perpendicular to the beam axis.

In the electron collection system, motion perpendicular to the beam axis is confined by a weak magnetic field parallel to the beam. The field is produced by a dc current flowing in a solenoid of copper wire insulated by glass fiber tubing. The solenoid is wound on a molybdenum tube of 2.5 cm inside diameter, through which the laser and ion beams pass. A grooved aluminum strip keeps the winding spacing uniform over most of the solenoid, but a closer spacing is provided at the entrance to compensate for end effects. At the end of the interaction region, the solenoid bends through a 5 cm radius toward a continuous-dynode electron multiplier. A reentrant tube of 1.25 cm diameter restricts the electrons entering the multiplier to those with a small cyclotron radius. In addition, electrons with high velocities experience curvature and gradient drifts²⁴ in the curved section and are lost. Operation of the solenoid at fields of ~ 10 G collects forward-emitted electrons with efficiency of about 40%, without energy discrimination. Reduction of the field to ~ 2 G causes fast electrons to be lost by giving them excessively large cyclotron radii and large gradient and curvature drifts. Threshold electrons are still collected with high efficiency at these reduced fields, however. In our present work, the solenoid was operated in this reduced-field mode, since it greatly suppressed the background due to processes producing fast electrons (≥ 10 meV), making the threshold and resonance features more prominent. This threshold enhancement occurs without loss of information on the total photodetachment cross section, since the total cross section is provided by the neutral channel signal.

C. Laser system

A versatile noncommercial cw dye laser²⁵ is used in these experiments. Using a linear cavity configuration, the laser is operated broadband (~ 1 cm⁻¹) with a birefringent filter, or narrowband (~ 1 GHz) with the addition of an etalon. Conversion to a ring cavity is convenient, and with the addition of a unidirectional device and Mach-Zehnder interferometer²⁶ (which selects a single cavity mode, as a thick etalon does in more conventional systems) the laser runs single mode. When very narrow linewidth is necessary (for example, when autodetachment linewidths are measured) a piezoelectrically driven mirror and intracavity galvo plate are added to the cavity and the laser is electronically stabilized to an external reference etalon. Electronic stabilization reduces the laser linewidth to less than 100 kHz, although velocity spread in the ion beam contributes a Doppler width of 20 MHz to the spectra. All experiments described in this paper are carried out with DCM dye, pumped with 3–4 W of light from an argon-ion laser operating on all lines. Broadband dye output is roughly 700 mW at the peak of the gain curve, while single-mode output is about 400 mW. Photodetachment signals are strong over most of the spectrum. Indeed, it is frequently necessary to reduce the ion beam current to prevent saturation of the detectors, as count rates often exceed hundreds of kHz.

The line shape of the laser is monitored by two Fabry-Perot etalons. Absolute wavelength calibration (to an accuracy of 0.01 cm⁻¹ or 1/4 of the laser linewidth, whichever is greater) is provided by a lambda-meter²⁷ (traveling Michelson interferometer) using a polarization-stabilized helium-neon laser reference.²⁸

D. Data acquisition

Spectra are accumulated by a PDP-11/23 computer system, which either scans the laser frequency or the ion beam velocity. Most spectra are accumulated by laser tuning, including the broadband and narrowband spectra. Over short scan intervals, the most accurate relative frequency measurements are obtained by velocity tuning,²² which varies the Doppler shift of the ion beam. Most linewidth measurements are accomplished by velocity tuning. The computer counts the number of electrons and neutrals detected, while measuring and normalizing to the ion current and laser power. The high signal rates allow us to shorten integration times at each point to 1 s, yielding signal-to-noise ratios better than 100:1 for most of the data.

III. RESULTS

A. Low resolution data

At 1 cm⁻¹ resolution, the data from the slow electron detector show many prominent features (Fig. 2), enhanced by the preferential detection of threshold electrons. These features are similar to the features seen in the earlier ion-cyclotron resonance work.⁴ The stronger features are also visible in the total cross section obtained from the neutral detector, although the accumulated background from the many channels opening at lower energies makes them less obvious. The positions, intensities, and vibrational assign-

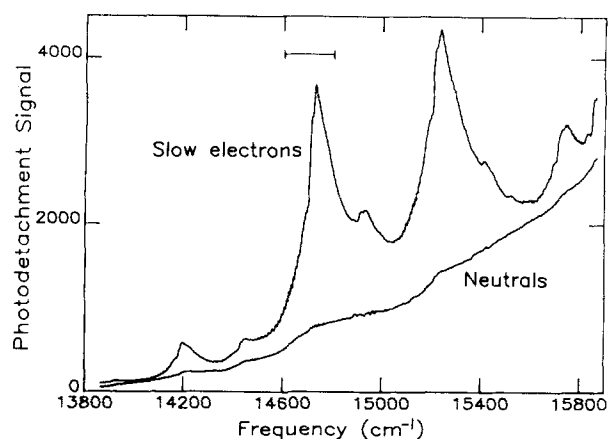


FIG. 2. Photodetachment signals from acetaldehyde enolate negative ion, taken with 1 cm^{-1} resolution. The upper curve shows the data from the slow electron detector, which enhances threshold and resonance features. The lower curve shows data from the neutral detector, which are representative of the total photodetachment cross section. The bracket shows the region expanded in Fig. 3.

ments of the features are given in Table I. The 0-0 transition was conclusively assigned in the earlier ICR work,⁴ since the position of the resonance with respect to the threshold for direct photodetachment did not shift upon deuteration. Strong features are observed for excitation of the C-C-O bending mode and for the C-C stretching mode, although the data do not reach far enough to the blue to observe the C-O stretching mode. Published photoelectron spectra²⁹ of the anion show prominent features corresponding to excitation of the radical bending mode, and very recently obtained photoelectron spectra³⁰ display features for several other modes. There is reasonable agreement between the vibrational frequencies measured in this work and those obtained from photoelectron spectra of the anion^{29,30} and from dispersed fluorescence studies³¹ of the radical. The precision of the values reported here is somewhat better, however. A prominent hot band gives the C-C-O bending frequency in the anion ground state.

Weak features are seen at positions 200 cm^{-1} to the blue of the strong features. A 200 cm^{-1} hot band has been observed by Inoue and Akimoto³¹ in their fluorescence exci-

TABLE I. Observed vibrational transitions.

Frequency (cm^{-1})	Modes ^a	Intensity
13 912	$3_1^0 4_1^1$	weak
14 185	3_1^0	medium
14 432	4_1^1	medium
14 710	0-0	strong
14 915	4_0^2	weak
14 935	$3_1^1 4_1^1$	weak
15 209	3_0^1	strong
15 410	$3_1^1 4_0^2$	weak
15 444	$3_0^2 4_1^1$	weak
15 711	3_0^2	strong
15 853	2_1^0	strong

^a Mode designations are $\omega_2 = \text{C-C stretch}$, $\omega_3 = \text{C-C-O bend}$, $\omega_4 = \text{torsion}$.

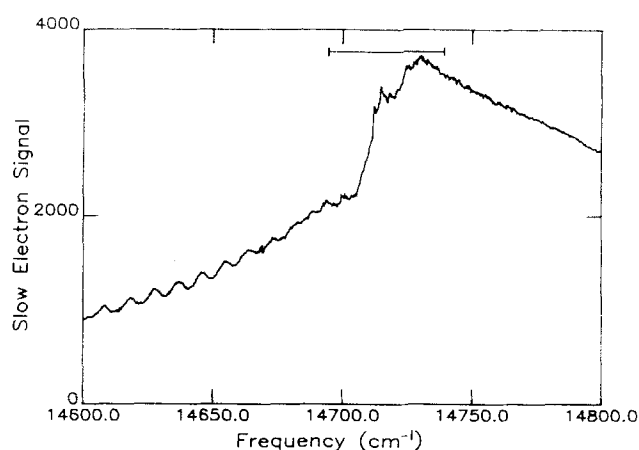


FIG. 3. Expanded view of the slow electron cross section near the 0-0 transition, at 1 cm^{-1} resolution. The bracket shows the region expanded in Fig. 4.

tation spectrum of the radical. It is likely that these 200 cm^{-1} features are due to an out-of-plane vibrational mode (species A'') of the radical, since no in-plane modes (species A') are expected to have such low frequencies. Out-of-plane modes can be excited from the ground state only to even vibrational levels,³² so the 200 cm^{-1} features would correspond to a mode with a 100 cm^{-1} vibrational frequency. *Ab initio* calculations¹⁹⁻²¹ find a low bond order for the C-C bond. From the analysis of the rotational spectrum described later in this paper, the bond length is found to be long, characteristic of a single bond. The low frequency mode might then be tentatively ascribed to the torsional mode in the radical. From infrared spectra ($400\text{--}4000 \text{ cm}^{-1}$) of the radical trapped in an argon matrix, Jacox³³ has deduced a frequency of 765 cm^{-1} for the torsional mode. This is not a likely assignment, since single-bond torsional frequencies are at most a few hundred wave numbers. Additional features appear 275 cm^{-1} to the red of the strong features, possibly due to 1-1 transitions in the torsional mode. This tentative assignment would yield a torsional frequency of about 375 cm^{-1} in the ground state of the anion.

An expanded view of the 0-0 transition is shown in Fig. 3. There is an obvious step in the cross section near $14 700 \text{ cm}^{-1}$, and striking undulations appear somewhat below this onset. Near the onset, these undulations become erratic and the spectrum at this resolution (still $\sim 1 \text{ cm}^{-1}$) appears noisy. Investigation at higher resolution shows incipient structure in these regions.

B. Medium resolution data

At this point it is appropriate to consider the signatures by which dipole-bound states may be recognized. At least one dipole-bound state of a molecule with moderate dipole moment ($2\text{--}4 \text{ D}$) will lie between zero and several tens of wave numbers below the ground neutral state.¹¹ The lower rotational levels of this state will be truly bound. Higher rotational levels will lie in the continuum, and may autodetach by rotation-electronic coupling. These levels will cause numerous resonances to be observable in the photodetachment cross section, near the threshold for direct photodetachment to the continuum. One need not search the entire

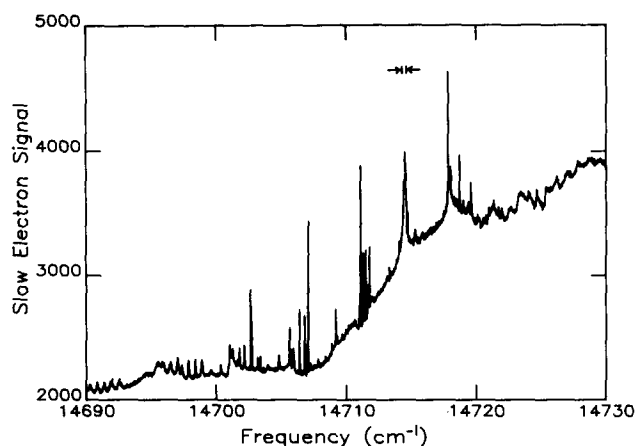


FIG. 4. Medium resolution (~ 1 GHz or 0.03 cm^{-1}) scan of the slow electron cross section near the $0-0$ threshold. The sharp resonances are due to excitation to dipole-bound levels, followed by autodetachment. The broadening of lines away from the band center is visible. The bracket shows the region expanded in Fig. 5.

spectrum to find dipole-bound states. Only the region near threshold need be studied, although the instrumental linewidth must be sufficiently narrow to resolve the resonances above the background.

The relevant region in acetaldehyde enolate was scanned with 1 GHz resolution to search for resonant structure. As shown in Fig. 4, numerous resonances were seen in the threshold electron channel in this region. Above and below this range, sharp structure was not observable. The presence of structure near threshold matches the expectations for a system supporting a dipole-bound state, but is not yet proof of such states. Such structure was not observed at thresholds for forming vibrationally excited products, but only broad, undifferentiated structure was seen. This suggests the presence of strong vibration-electronic coupling.

C. High resolution data

To elucidate further the nature of the states involved in the resonances, the laser was operated single mode, giving data from the photodetachment spectrometer at its Doppler-limited resolution of 20 MHz (0.0007 cm^{-1}). A sample of these threshold electron data is shown in Fig. 5(a), where now individual rotational transitions are fully resolved. Note that this represents a scale expansion by a factor of 10^4 over the data of Fig. 2. The positions of many lines were measured sufficiently well to allow spectroscopic assignment. Table II shows their observed frequencies, labeled by the usual notation J_{K_a, K_c} . Most were directly observed as autodetaching features; a few were observable only if an electric field was applied after excitation. The role of the electric field will be discussed in Sec. III F. Assignment of the lines was achieved by consideration of an appropriate model for the transitions.

The rotational energy levels of the negative ion states may be described by a simple near-prolate asymmetric top model.³² Levels in the ground valence state and upper negative ion state are labeled by rotational angular momentum N (equivalent to total angular momentum J in this case) and angular momentum projection onto the axis of least moment of inertia K_a . These zero-order levels are split into pairs in all

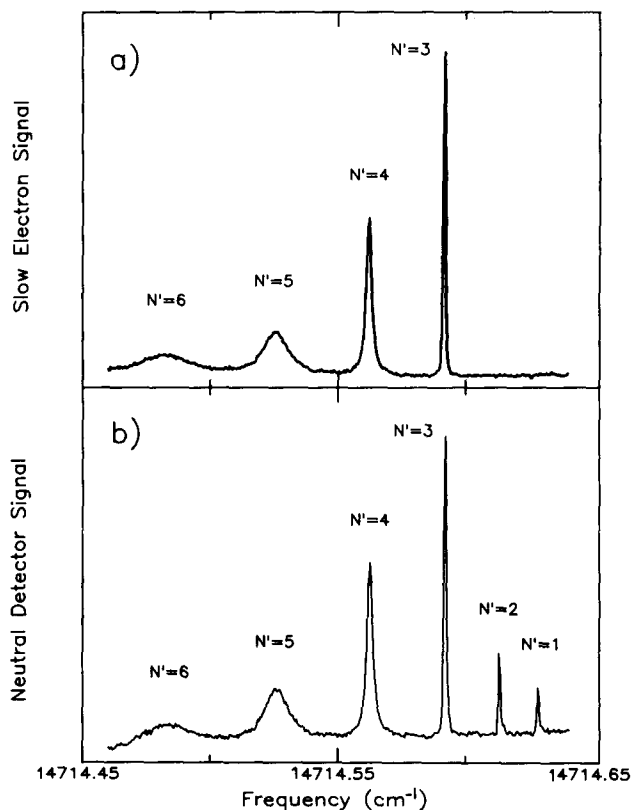


FIG. 5. High resolution scan (20 MHz or 0.0007 cm^{-1}) of the $K_a = 1 \leftarrow K_a = 0$ Q branch, showing the variation of width with rotational excitation in the upper state. (a) The cross section as measured by the slow-electron detector, which is essentially field free. (b) The data from the neutral detector, which follows a region where electric-field-induced detachment of weakly bound levels takes place.

but the $K_a = 0$ levels due to the asymmetry of the molecule. The energy levels for asymmetric rotors may be found from perturbation expansions,^{32,34,35} but the most straightforward method³⁶ is to expand the asymmetric top wave function in a prolate top basis, and diagonalize the matrix containing the interaction between states of different K_a for a given J . Centrifugal distortion terms were not included in the Hamiltonian since only very low angular momentum states were observed.

Only transitions with $\Delta K_a = \pm 1$ were observed in the spectra, which would show features with intensities as little as 2% of the most intense lines. More asymmetric molecules would be expected to display other transitions in addition to these, but these states are sufficiently symmetric to make such transitions very weak. The limitation to $\Delta K_a = \pm 1$ transitions indicates that the electronic transition moment is perpendicular to the a axis. Furthermore, the nature of transitions between asymmetry doublets shows the transition moment to be along the c axis, i.e., perpendicular to the molecular plane.³² Thus, the transition occurs between states belonging to the two different representations of the symmetry group of the molecule. Electronic structure calculations¹⁹ find the anion ground state to be A' , and the dipole-bound state to be A'' , consistent with these results.

The data for each species were entered into a nonlinear least-squares program³⁷ which fitted the line positions to

TABLE II. Line positions for rotational transitions from ground ion state to dipole-bound state, corrected for the ion beam Doppler shift. Levels are labeled by J_{K_a, K_c} . One-sigma measurement errors are roughly 0.01 cm^{-1} . Lines too broad for accurate measurement are not included. There were no unassigned lines. Asterisks denote lines observed only by field detachment (see Sec. III F).

Upper level	Lower level	Frequency (cm^{-1})	Upper level	Lower level	Frequency (cm^{-1})	Upper level	Lower level	Frequency (cm^{-1})
H_2CCHO^-								
0 ₀₀	1 ₁₀	14 709.895*	4 ₁₄	5 ₂₄	14 702.520	4 ₁₄	4 ₀₄	14 714.525
1 ₀₁	1 ₁₁	14 710.640*	5 ₁₅	4 ₂₃	14 709.240	4 ₁₃	5 ₀₅	14 711.712
2 ₀₂	2 ₁₂	14 710.728*	5 ₁₅	5 ₂₃	14 705.831	5 ₁₄	4 ₀₄	14 718.720
3 ₀₃	3 ₁₃	14 710.804*	5 ₁₅	6 ₂₅	14 701.790	5 ₁₅	5 ₀₅	14 714.496
4 ₀₄	3 ₁₂	14 713.350	6 ₁₆	6 ₂₄	14 705.750	5 ₁₄	6 ₀₆	14 711.286
4 ₀₄	4 ₁₄	14 711.020	7 ₁₇	7 ₂₅	14 705.619	6 ₁₅	5 ₀₅	14 719.660
4 ₀₄	5 ₁₄	14 707.037	3 ₁₂	3 ₂₂	14 706.273	6 ₁₆	6 ₀₆	14 714.463
5 ₀₅	4 ₁₃	14 714.010	4 ₁₃	3 ₂₁	14 709.160	6 ₁₅	7 ₀₇	14 710.905
5 ₀₅	5 ₁₅	14 711.188	4 ₁₃	4 ₂₃	14 706.462	7 ₁₇	7 ₀₇	14 714.410
5 ₀₅	6 ₁₅	14 706.287	4 ₁₃	5 ₂₃	14 703.050	2 ₂₀	3 ₃₀	14 698.850
6 ₀₆	5 ₁₄	14 714.622	5 ₁₄	5 ₂₄	14 706.685	2 ₂₁	3 ₃₁	14 698.850
6 ₀₆	6 ₁₆	14 711.394	5 ₁₄	6 ₂₄	14 702.560	3 ₂₁	4 ₃₁	14 698.267
6 ₀₆	7 ₁₆	14 705.547	6 ₁₅	5 ₂₃	14 710.960	3 ₂₂	4 ₃₂	14 698.267
7 ₀₇	8 ₁₇	14 704.717	6 ₁₅	6 ₂₅	14 706.964	4 ₂₂	5 ₃₂	14 697.637
3 ₁₃	2 ₂₁	14 707.960	6 ₁₅	7 ₂₅	14 702.100	4 ₂₃	5 ₃₃	14 697.637
3 ₁₃	3 ₂₁	14 705.937	1 ₁₁	1 ₀₁	14 714.593*	5 ₃₂	4 ₄₀	14 698.806
3 ₁₃	4 ₂₃	14 703.240	2 ₁₂	2 ₀₂	14 714.579*	5 ₃₃	4 ₄₁	14 698.806
4 ₁₄	3 ₂₂	14 708.620	3 ₁₃	3 ₀₃	14 714.550			
4 ₁₄	4 ₂₂	14 705.893	4 ₁₃	3 ₀₃	14 717.780			
D_2CCDO^-								
5 ₀₅	5 ₁₅	14 665.27	4 ₁₃	4 ₂₃	14 662.48	6 ₁₆	6 ₂₄	14 661.56
5 ₀₅	6 ₁₅	14 660.79	4 ₁₃	5 ₂₃	14 659.51	6 ₁₆	7 ₂₆	14 657.61
6 ₀₆	6 ₁₆	14 665.47	5 ₁₄	5 ₂₄	14 662.69	7 ₁₇	7 ₂₅	14 661.34
6 ₀₆	7 ₁₆	14 660.04	6 ₁₅	6 ₂₅	14 662.98	7 ₁₇	8 ₂₇	14 656.91
7 ₀₇	7 ₁₇	14 665.62	6 ₁₅	7 ₂₅	14 658.69	8 ₁₈	9 ₂₈	14 656.17
7 ₀₇	8 ₁₇	14 659.25	7 ₁₆	7 ₂₆	14 663.29	9 ₁₉	10 ₂₉	14 655.44
8 ₀₈	8 ₁₈	14 665.83	7 ₁₆	8 ₂₆	14 658.29	2 ₂₀	3 ₃₀	14 657.38
8 ₀₈	9 ₁₈	14 658.41	8 ₁₇	8 ₂₇	14 663.60	2 ₂₁	3 ₃₁	14 657.38
4 ₁₃	5 ₀₅	14 664.69	8 ₁₇	9 ₂₇	14 657.83	3 ₂₁	4 ₃₁	14 656.85
5 ₁₄	6 ₀₆	14 664.38	4 ₁₄	3 ₂₂	14 664.19	3 ₂₂	4 ₃₂	14 656.83
4 ₁₄	4 ₀₄	14 666.94	4 ₁₄	4 ₂₂	14 661.85	4 ₂₂	5 ₃₂	14 656.35
5 ₁₅	5 ₀₅	14 666.89	4 ₁₄	5 ₂₄	14 658.95	4 ₂₃	5 ₃₃	14 656.31
6 ₁₆	6 ₀₆	14 666.84	5 ₁₅	4 ₂₃	14 664.69	5 ₂₃	6 ₃₃	14 655.87
7 ₁₇	7 ₀₇	14 666.79	5 ₁₅	5 ₂₃	14 661.71	5 ₂₄	6 ₃₄	14 655.77
8 ₁₈	8 ₀₈	14 666.74	5 ₁₅	6 ₂₅	14 658.29	6 ₂₄	7 ₃₄	14 655.44

seven parameters; the band origin, and the rotational constants A , B , and C for each of the two states. Energies were computed for the rigid asymmetric top model using the matrix method³⁶ described earlier. The resulting constants with their associated error limits are displayed in Table III. No

TABLE III. Spectroscopic constants obtained from least-squares fitting the data of Table II.

Constant	$\text{H}_2\text{CCHO}^-^a$ (cm^{-1})	$\text{D}_2\text{CCDO}^-^a$ (cm^{-1})
A'	2.219(0.003)	1.419(0.003)
B'	0.3758(0.0004)	0.3302(0.0003)
C'	0.3207(0.0003)	0.2680(0.0003)
Δ'^b	0.110(0.08)	-0.030(0.08)
A''	2.493(0.0013)	1.554(0.0012)
B''	0.3622(0.0003)	0.3192(0.0002)
C''	0.3159(0.0004)	0.2639(0.0004)
Δ''^b	0.060(0.07)	0.013(0.07)
ν_0	14 712.742(0.05)	14 665.966(0.05)
σ^c	0.014	0.010

^a Values in parentheses are one standard error.

^b Δ is the inertial defect, $I_c - I_b - I_a$ in $\text{amu } \text{\AA}^2$.

^c Standard deviation of fit.

strong correlations were found in the residuals of the fits. All lines for which precise positions could be measured (55 lines in H_2CCHO^- , 45 lines in D_2CCDO^-) were included in the fits. There were no unassigned lines. The standard deviations of the residuals were approximately equal to the 0.01 cm^{-1} random error in wavelength measurement.

D. Molecular structure

The constants provide information about the structure of the molecule. One measure of possible nonplanarity is provided by the "inertial defect." Planar species with principal moments of inertia I_a , I_b , and I_c ideally obey the relation $I_c = I_b + I_a$. Molecular vibration causes slight deviations from this rule, although calculation³⁸ of these effects requires knowledge of the force field for the molecule. Nevertheless, the ideal relation is satisfied (within our experimental error) for both states of both species studied. The results are therefore consistent with planar structures for radical and anion.

If the electron does not significantly perturb the core, then the geometry of the dipole-bound state should be nearly identical to that of the neutral. This will be reflected in their

TABLE IV. Rotational constants for H_2CCHO , obtained from least-squares fitting B and C , assuming planarity of the molecule to compute A .

Constant	Anion dipole-bound state ^a (cm^{-1})	Neutral radical ^{a, b} (cm^{-1})
A	2.218(0.0023)	2.228(0.012)
B	0.3756(0.0003)	0.3809(0.001)
C	0.3212(0.0003)	0.3253(0.001)

^a Values in parentheses are one standard error.

^b Reference 39.

rotational constants, which should also be very similar. Very recent laser induced fluorescence studies³⁹ of the radical in a free jet expansion have provided the rotational constants of the neutral radical. The constants from that study were obtained from fits where the inertial defect was set at zero, so we did an additional fit of our data imposing this condition. The comparison is presented in Table IV. There is remarkable similarity between the values for the upper negative ion state and those for the neutral radical. This confirms that the extra electron in the upper negative ion state does not substantially perturb the core, a characteristic which differentiates dipole-bound states from valence states. The constants do, however, differ by a statistically significant amount. The moments of inertia for the excited anion are slightly greater than those for the radical. While this difference could be ascribed entirely to a slight change in geometry (a shift of ~ 0.002 Å in atomic positions), it may also reflect the presence of the electron at a large distance (~ 40 Å) from the core, giving a (relatively) large moment for the light particle. Since the source of the changes in spectroscopic constants is uncertain, we have not attempted to determine the geometry change precisely.

Calculations by Garrett¹¹ of dipole-bound rotational levels of diatomic molecules show highly anomalous rotational energy levels, which do not reflect the usual $J(J+1)$ dependence of energy levels in diatomic molecules. While acetaldehyde enolate differs qualitatively from these systems, it is still surprising that the rotational levels of its dipole-bound state are so regular. We hope this question can be resolved by experimental studies on the rotational structure of diatomic molecules.²

Since only two isotropic variants were studied, the positions of all atoms in the molecules cannot be determined from the data. Sufficient information exists in the data to determine the positions of the heavy atoms if the positions of the hydrogens are assumed. The positions for hydrogen atoms in the radical are obtained from *ab initio* calculations,^{20,21} while those for the anion are based upon measured values in neutral species of similar electronic structure. Of course, zero-point vibration causes⁴⁰ the effective hydrogen and deuterium bond lengths to differ, and they will be about 0.01 Å longer than the equilibrium values. In these calculations, the isotope effects were neglected, but 0.01 Å was added to the equilibrium values obtained from theory. Least-squares fitting of the raw data (line positions) was carried out, but the two data sets (for the hydrogenated and for the deuterated species) were fitted simultaneously. The fitting

TABLE V. Geometric parameters of the ground state and dipole-bound state. Atoms are labeled according to Fig. 6.

Parameters	Ground state anion ^a	Dipole-bound state ^a
Fitted		
$R(\text{C}_1\text{C}_2)$	1.324(0.019)	1.391(0.021)
$R(\text{C}_2\text{O})$	1.334(0.019)	1.298(0.022)
$\angle(\text{C}_1\text{C}_2\text{O})$	129.4(0.025)	123.1(0.09)
Fixed		
$R(\text{C}_1\text{H}_1)$	1.100	1.082
$R(\text{C}_1\text{H}_2)$	1.090	1.080
$R(\text{C}_2\text{H}_3)$	1.100	1.093
$\angle(\text{H}_1\text{C}_1\text{C}_2)$	120.0	119.6
$\angle(\text{H}_2\text{C}_1\text{C}_2)$	121.0	121.2
$\angle(\text{H}_3\text{C}_2\text{C}_1)$	116.0	118.4

^a Bond lengths are in angstroms, angles in degrees. One standard deviation statistical errors, without account of possible inaccuracies of the fixed parameters, are given in parentheses.

procedure adjusted the band origins for acetaldehyde enolate- h_3 and $-d_3$, and the C–C and C–O bond lengths and C–C–O angle for each state, for a total of eight parameters. The results of this fit, and the positions assumed for the hydrogens, are shown in Table V. Figure 6 shows the geometry of the dipole-bound state and the direction of the dipole moment in the radical. The C–C–O angle is well determined from the fitting, and is not particularly sensitive to the choice of hydrogen positions. The bond lengths obtained are not so precise, due to a strong inverse correlation between the C–C and C–O bond length and strong dependence upon the choice of hydrogen positions. Nevertheless, the results show clearly the changes in bond order expected for the transition. The ground state has a short C–C distance (1.32 Å), close to the typical value of 1.34 Å for a double bond. The C–O bond length of 1.33 Å is shorter than a C–O single bond (~ 1.43 Å) but significantly longer than a double bond (~ 1.23 Å). This reflects the low C–O bond order for this state where the extra charge is localized on the oxygen atom. The excited state shows the opposite characteristics: the carbon–carbon bond

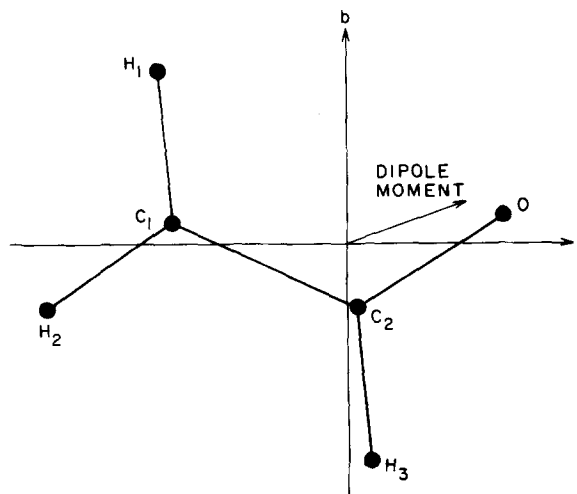


FIG. 6. The dipole-bound state of acetaldehyde enolate, showing the placement of principal axes and the direction (Ref. 20) of the dipole moment of the neutral radical.

lengthens to 1.39 Å, with a bond order between one and two. The C–O bond contracts to 1.30 Å, more closely resembling a double bond.

E. Linewidths and lifetimes

The rotational spectrum of the transition from the ground state to excited anion state was found to be amazingly simple. A usual bound state to bound state transition in such an asymmetric top would have given rise to thousands of spectral lines, but less than one hundred sharp lines were visible in our data. The spectral simplification is due to the extremely broad linewidth of transitions to higher rotational levels in the excited state. Levels with rotational quantum number N greater than seven were not readily identifiable in the spectrum of acetaldehyde enolate- h_3 , and $N = 9$ was the upper limit in the spectrum of the $-d_3$ compound. Beyond these limits, the lines became so broad that they could not be distinguished from the background due to direct photodetachment. Furthermore, the lowest few levels were missing from the spectra. The consistent variation of linewidth with rotational quantum number (see, for example, Fig. 5) simplified the initial assignment of the spectra, since a line was “tagged” by its linewidth as to its approximate upper state rotational quantum number. Vestiges of the high rotational levels remain, as evidenced by the “ripples” in Fig. 3 below $14\,700\text{ cm}^{-1}$. These are due to clusters of $\Delta K_a = -1$ transitions to levels of high J and K_a . For example, the last ripple at the extreme left in Fig. 3 corresponds to $K'_a = 12 \leftarrow K''_a = 13$. Because the rotational constant A is smaller in the upper state than in the lower state, an r -form head of lines with $\Delta K_a = +1$ forms in the $14\,750\text{ cm}^{-1}$ region.

The widths of many lines were measured with the highest resolution available. Different transitions terminating in the same upper state were observed to have identical linewidths. The line shapes, when not limited by our resolution of 20 MHz (0.0007 cm^{-1}) were Lorentzian. Fano profiles are not expected in these types of systems,²² since the background is due to a great many open continuum channels, and a particular transition cannot interfere with most of them. The results from fitting the lines to a Lorentzian function are summarized in Table VI.

In the acetaldehyde enolate- h_3 , levels with $N' \leq 3$ in $K'_a = 0$ and $N' \leq 2$ in $K'_a = 1$ are not seen. More lines are missing in the acetaldehyde enolate- d_3 ; $N' \leq 4$ in $K'_a = 0$, and $N' \leq 3$ in $K'_a = 1$ are not observed. Furthermore, different members of the asymmetry doublets in $K'_a = 1$ show different widths. While there is a general tendency for widths to increase with rotational energy, the upper level of an asymmetry doublet is often narrower than the lower level. A simple phase-space law without selection rules cannot explain these results. The selection rules required to explain the observed spectra are developed below.

Any autodetachment process must conserve energy and angular momentum. The rotational angular momenta N for the autodetaching state and for the neutral radical must satisfy the triangular conditions with the electron orbital angular momentum. For a molecule with light atoms, spin-orbit coupling will be weak, and the spin-rotation coupling in the final state radical³⁹ is small for low rotational levels.

The symmetry of the electronic and rotational wave functions must also be considered. For a planar asymmetric top, two treatments are possible. Mulliken⁴¹ showed that by considering the point group for the asymmetric top wave functions D_2 and including the behavior under inversion, the proper selection rules for rotational transitions may be derived. A more powerful and general technique was developed by Hougen,⁴² whose theory considers the full symmetry of the rovibronic wave function. Hougen's method applied in this case classifies the wave function according to representations of the group D_{2h} .

A transition will be allowed if the direct product of the representations for the autodetaching state, neutral state, and continuum electron contains the totally symmetric representation. The representations for the rotational levels are easily obtained from their quantum numbers.^{32,36,41} The electronic symmetry under reflection in the molecule-fixed frame translates into inversion symmetry in the space-fixed frame. Thus, transitions which would be allowed by energy and angular momentum conservation may be forbidden by parity conservation. Several transitions with $\Delta N = -1$ must therefore proceed by emission of a d wave, for instance, because a p wave would not conserve parity.

TABLE VI. Full widths of autodetaching lines in MHz. Errors are approximately 10%.

J	$K_a = 0$	$K_a = 1, K_c = J - 1^a$	$K_a = 1, K_c = J^b$	$K_a = 2^c$
0	Bound
1	Bound	Bound	Bound	...
2	Bound	Bound	Bound	1100
3	Bound	< 20 ^d	< 20	1500
4	< 20	< 25	50	1900 ^e
5	100	140	275	2900 ^e
6	330	510	510	
7	1200	1200	1200	Very broad

^a Upper level of asymmetry doublet.

^b Lower level of asymmetry doublet.

^c Both K_c levels have similar width.

^d $J = 3, K_a = 1, K_c = 2$ is very weak. We believe its lifetime is comparable to the transit time or fluorescence time.

^e Asymmetry doubling not resolved, but is 500 and 1300 MHz for $J = 4$ and 5, respectively, so these values are somewhat high.

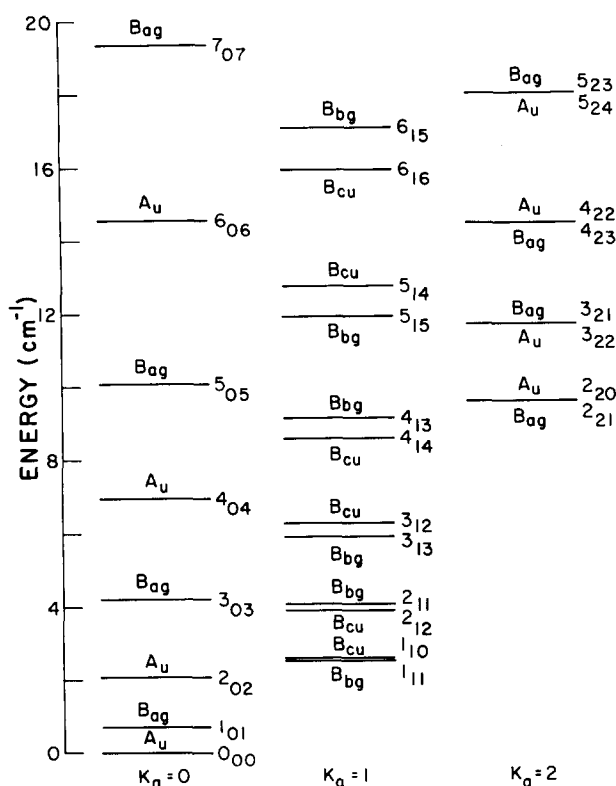


FIG. 7. Energy levels of the dipole-bound state, with symmetry designations of the group D_{2h} .

The energetics of the autodetachment may be studied by using the rotational energies for the excited anion state determined here, and the energies determined by laser-induced fluorescence studies³⁹ for the radical. The binding energy of the excited anion state may be adjusted to obtain correspondence with the observed autodetachment data. Obviously, the 3_{13} excited anion level is above the 0_{00} radical level, since it autodetaches. This requires the binding energy E_b to be less than 5.9 cm^{-1} . We suggest the highest level not seen, 3_{03} , is below the onset of any continuum, yielding $E_b > 4.1 \text{ cm}^{-1}$. The energies and symmetries of the dipole-bound state levels are shown in Fig. 7. While it is enticing to attempt to determine the binding energy more closely by analysis of the linewidths and possible autodetachment channels, it appears that the dynamics are too complex and the data too few to make this process reliable. In any case, we present in Table VII some of the probable channels and the binding energies at which they become allowed. The parity selection rules are seen to be the likely influence causing the upper levels of the $K'_a = 1$ asymmetry doublets to be long lived.

F. Field detachment

Transitions to levels bound with respect to autodetachment do not appear in the spectra taken with the slow electron detector, since they can only fluoresce back to the ground state and do not produce electrons. Ions excited to these levels may have sufficient lifetimes to exit the slow electron collector and enter the second quadrupole deflector while still in the excited state. The deflector²³ uses a strong

TABLE VII. Probable channels for autodetachment of the dipole-bound state, showing binding energy at which channel opens. Levels designated by $N_{K_a K_c}$.

Dipole-bound state	Radical state	Electron wave	Maximum binding energy (cm^{-1})
$3_{13}(B_{2g})$	$1_{01}(B_{1g})$	$d(B_{3g})$	5.2
	$0_{00}(A_u)$	$f(B_{2u})$	5.9
$3_{12}(B_{3u})$	$1_{01}(B_{1g})$	$f(B_{2u})$	5.5
	$0_{00}(A_u)$	$g(B_{3g})$	7.0
$4_{14}(B_{3u})$	$3_{03}(B_{1g})$	$p(B_{2u})$	4.4
	$2_{12}(B_{3u})$	$d(A_g)$	4.7
	$2_{02}(A_u)$	$d(B_{3g})$	6.5
$4_{13}(B_{2g})$	$3_{03}(B_{1g})$	$d(B_{3g})$	4.9
	$2_{11}(B_{3g})$	$d(A_g)$	5.1
	$2_{02}(A_u)$	$f(B_{2u})$	7.0
$5_{15}(B_{2g})$	$4_{04}(A_u)$	$p(B_{2u})$	4.9
	$3_{13}(B_{2g})$	$d(A_g)$	6.0
	$3_{03}(B_{1g})$	$d(B_{3g})$	7.8
$5_{14}(B_{3u})$	$4_{04}(A_u)$	$d(B_{3g})$	5.8
	$3_{12}(B_{3u})$	$d(A_g)$	6.5
$4_{04}(A_u)$	$2_{02}(A_u)$	$d(A_g)$	4.9
	$1_{01}(B_{1g})$	$f(B_{1u})$	6.3
$5_{05}(B_{1g})$	$3_{03}(B_{1g})$	$d(A_g)$	6.2
$6_{06}(A_u)$	$4_{04}(A_u)$	$d(A_g)$	7.6
$7_{07}(B_{1g})$	$6_{06}(A_u)$	$p(B_{1u})$	4.8
	$5_{05}(B_{1g})$	$d(A_g)$	8.9

transverse electric field to separate the primary negative ion beam from the neutral photodetachment products. Ground state ions are simply deflected into a Faraday cup. Dipole-bound states of the anion are so diffuse and weakly bound that the electric field rapidly detaches the electron, and the neutral thus formed proceeds into the neutral detector. Thus, while transitions to the autodetaching levels are detected in both the electron and neutral channels, transitions to stable levels of the excited anion state appear only in the neutral channel (Fig. 5). Attempts were made to measure the minimum field required to detach the ions. The potentials on the second quadrupole deflector were reduced substantially, but could not be reduced sufficiently to avoid field detachment. In the present configuration of our apparatus, the primary ion beam strikes the neutral detector at fields below 70 V/cm ; this value was only achieved after the ion beam energy was reduced to 1 keV . At present then, we can only report that fields of 70 V/cm or less are capable of causing detachment from the lowest dipole-bound states. This suggests the electron wave function reaches hundreds of angstroms from the core.⁴³

IV. CONCLUSIONS

High-resolution photodetachment spectroscopy has made possible detailed characterization of the structure and energetics of an unusual electronic state in acetaldehyde enolate, and provided clues as to the dynamics of electron loss from rotationally excited levels. The results presented here demonstrate the existence of an anion state in which the extra electron is very slightly bound ($\sim 5 \text{ cm}^{-1}$) with respect to the neutral radical. Examination of the moments of inertia reveals that the electron has almost no effect upon the structure of the core. Since very weak electric fields are sufficient

to detach the electron from the core, this electron must lie in a very diffuse orbital. These unusual attributes are characteristic of diffuse dipole-bound anions, in which the electron has large mean radius,⁴⁴ is weakly bound, and has very little effect upon the core. The extra electron is bound by the electric dipole field of the neutral radical.

Dipole-bound states are qualitatively different from conventional valence states. They will be present whenever a molecule has a moderately large dipole moment. Many systems, then, are available for their study. The similarities to Rydberg states of neutrals provide a partial framework in which to understand their properties. In many ways, however, their characteristics differ dramatically from those of Rydbergs. The unique structure of dipole-bound states provides a valuable environment for the extension of our understanding of molecular physics.

ACKNOWLEDGMENTS

The successful completion of this work was facilitated by help from and consultation with many individuals. Peter Schulz carried out part of the design of the electron collection system. We are grateful to W. R. Garrett, A. R. P. Rau, W. P. Reinhardt, G. B. Ellison, K. Leopold, S. E. Novick, S. R. Leone, and S. V. O'Neil for helpful discussions. We thank T. A. Miller and his co-workers for communicating their results prior to publication. The assistance of J. L. Hall and L. Hollberg with the design and construction of the laser system is gratefully acknowledged. C. V. Kunasz and J. Levine provided valuable computational assistance, and D. Hendry and H. Rohner fabricated the electron collection system. J. Marks acknowledged the support of an Exxon graduate fellowship. Support for this research was provided by the National Science Foundation under Grants CHE83-16628, PHY82-00805, CHE78-21064, and CHE83-13333.

¹K. R. Lykke, R. D. Mead, and W. C. Lineberger, *Phys. Rev. Lett.* **52**, 2221 (1984).

²Dipole-bound states have recently been observed in FeO⁻ by K. R. Lykke and D. Neumark working at JILA. Their results will appear in a subsequent paper.

³A. H. Zimmerman and J. I. Brauman, *J. Chem. Phys.* **66**, 5823 (1977); R. L. Jackson, A. H. Zimmerman, and J. I. Brauman, *ibid.* **71**, 2088 (1979).

⁴R. L. Jackson, P. C. Hiberty, and J. I. Brauman, *J. Chem. Phys.* **74**, 3705 (1981).

⁵W. R. Garrett, *Chem. Phys. Lett.* **5**, 393 (1970); W. R. Garrett, *Phys. Rev. A* **3**, 961 (1971).

⁶E. Fermi and E. Teller, *Phys. Rev.* **72**, 406 (1947).

⁷A. S. Wightman, *Phys. Rev.* **77**, 521 (1950).

⁸J. E. Turner and K. Fox, *Phys. Lett.* **23**, 547 (1966); W. B. Brown and R. E. Roberts, *J. Chem. Phys.* **46**, 2006 (1967); M. H. Mittelman and R. E. von Holdt, *Phys. Rev.* **140**, 726 (1965); J.-M. Levy-Leblond, *ibid.* **153**, 1 (1967). A good review of the problem is provided by J. E. Turner, *Am. J. Phys.* **45**, 758 (1977).

⁹C. A. Coulson and M. Walmsley, *Proc. Phys. Soc.* **91**, 31 (1967); O. H. Crawford, *ibid.* **91**, 279 (1967).

¹⁰W. R. Garrett, in *Physics of Electronic and Atomic Collisions*, edited by S. Datz (North-Holland, Amsterdam, 1982), pp. 65–77.

¹¹W. R. Garrett, *J. Chem. Phys.* **73**, 5721 (1980); **77**, 3666 (1982).

¹²K. D. Jordan and W. Luken, *J. Chem. Phys.* **64**, 2760 (1976).

¹³K. D. Jordan and J. J. Wendoloski, *Chem. Phys.* **21**, 145 (1977); K. D. Jordan and R. Seeger, *Chem. Phys. Lett.* **54**, 320 (1978); K. D. Jordan and J. J. Wendoloski, *Mol. Phys.* **35**, 223 (1978); B. Liu, K. O-Ohata, and K. Kirby-Docken, *J. Chem. Phys.* **67**, 1850 (1977); E. A. McCullough, *ibid.* **75**, 1579 (1981); L. Adamowicz and E. A. McCullough, *Chem. Phys. Lett.* **107**, 72 (1984).

¹⁴J. L. Carlsten, J. R. Peterson, and W. C. Lineberger, *Chem. Phys. Lett.* **37**, 5 (1976).

¹⁵S. F. Wong and G. J. Schulz, *Phys. Rev. Lett.* **33**, 134 (1974).

¹⁶K. Rohr and F. Linder, *J. Phys. B* **9**, 2521 (1976).

¹⁷K. Rohr, *J. Phys. B* **10**, 1175 (1977); G. J. Verhaart, W. J. Van der Haart, and H. H. Brongersma, *Chem. Phys.* **34**, 161 (1978).

¹⁸W. Domcke, L. S. Cederbaum, and F. Kaspar, *J. Phys. B* **12**, L359 (1979); W. Domcke and L. S. Cederbaum, *ibid.* **14**, 149 (1980).

¹⁹R. W. Wetmore, H. F. Schaefer III, P. C. Hiberty, and J. I. Brauman, *J. Am. Chem. Soc.* **102**, 5470 (1980).

²⁰E. S. Huyser, D. Feller, W. T. Borden, and E. R. Davidson, *J. Am. Chem. Soc.* **104**, 2956 (1982).

²¹M. Dupuis, J. J. Wendoloski, and W. A. Lester, *J. Chem. Phys.* **76**, 488 (1982).

²²U. Hefter, R. D. Mead, P. A. Schulz, and W. C. Lineberger, *Phys. Rev. A* **28**, 1429 (1983).

²³H. D. Zeman, *Rev. Sci. Instrum.* **48**, 1079 (1977).

²⁴J. D. Jackson, *Classical Electrodynamics* (Wiley, New York, 1975).

²⁵L. Hollberg and J. L. Hall (private communication).

²⁶J. C. Bergquist and L. Burkins, *Opt. Commun.* **50**, 379 (1984).

²⁷S. A. Lee and J. L. Hall, *Appl. Phys. Lett.* **25**, 367 (1976).

²⁸R. Balhorn, H. Kunzmann, and F. Lebowsky, *Appl. Opt.* **11**, 742 (1972).

²⁹G. B. Ellison, P. C. Engelking, and W. C. Lineberger, *J. Phys. Chem.* **86**, 4873 (1982).

³⁰D. G. Leopold, K. K. Murray, and W. C. Lineberger (in preparation).

³¹G. Inoue and H. Akimoto, *J. Chem. Phys.* **74**, 425 (1981).

³²G. Herzberg, *Electronic Spectra of Polyatomic Molecules* (Van Nostrand, New York, 1967).

³³M. E. Jacox, *Chem. Phys.* **69**, 407 (1982).

³⁴S. R. Polo, *Can. J. Phys.* **35**, 880 (1957).

³⁵C. H. Townes and A. L. Schawlow, *Microwave Spectroscopy* (Dover, New York, 1955).

³⁶G. W. King, R. M. Hainer, and P. C. Cross, *J. Chem. Phys.* **11**, 27 (1943).

³⁷C. Kunasz, program NLH05 (private communication).

³⁸T. Oka and Y. Morino, *J. Mol. Spectrosc.* **6**, 472 (1961); M. Nakata, K. Kuchitsu, and I. M. Mills, *J. Phys. Chem.* **88**, 344 (1984).

³⁹L. F. DiMauro, M. Heaven, and T. A. Miller, *J. Chem. Phys.* **81**, 2339 (1984).

⁴⁰W. Gordy and R. L. Cook, *Microwave Molecular Spectra* (Wiley-Interscience, New York, 1970).

⁴¹R. S. Mulliken, *Phys. Rev.* **59**, 873 (1941).

⁴²J. T. Hougen, *J. Chem. Phys.* **37**, 1433 (1962); **39**, 358 (1963).

⁴³In analogy with field ionization of Rydberg atoms and molecules [C. J. Latimer, *Contemp. Phys.* **20**, 631 (1979)], we may estimate the outermost extent r_{max} of the bound electron. Treating the dipole field as isotropic, we set the potential $V = -Er - eD/r^2$. Using the dipole moment D , the electric field E , and finding the barrier top where $dV/dr = 0$, we obtain $r_{\text{max}} \approx 700 \text{ \AA}$.

⁴⁴A crude estimate of the size of the bound electron's orbital may be obtained from setting $eD/r^2 = E_b$, where D is the dipole moment, and E_b is the binding energy. This gives a mean electron radius r of about 125 \AA .